Structures 63 (2024) 106421

Contents lists available at ScienceDirect

Structures

journal homepage: www.elsevier.com/locate/structures

Monte Carlo analysis of masonry structures under tsunami action: Reliability of lognormal fragility curves and overall uncertainty prediction

Maria Concetta Oddo [a], Panagiotis G. Asteris [b], Liborio Cavaleri [a,*]

[a] Department of Engineering, University of Palermo, Italy
[b] School of Pedagogical and Technological Education, Athens, Greece

ARTICLE INFO

Keywords:
Tsunami actions
Monte Carlo simulation
Fragility
Tsunami fragility functions
Uncertainties

ABSTRACT

Tsunami vulnerability of coastal buildings has gained more and more interest in recent years, in the consciousness of what losses may be caused. The improvement of the available approaches for the quantitative estimation of the probability of building damage and for defining possible strategies for risk mitigation is an actual goal. In this framework, several authors have provided empirical fragility curves based on field surveys after tsunamis. Nevertheless, a predictive approach based on analytical fragility curves, which can be extended to many classes of buildings, is essential for the scopes of civil protection and risk mitigation. In this paper, an approach for the construction of fragility curves, proposed for masonry structures under tsunami waves, is discussed and refined in the part regarding the assignment of the uncertainties. Further, an assessment of the reliability of the lognormal fragility distribution is carried out based on a Monte Carlo simulation applied to 4 classes of buildings. Here, it is shown that Monte Carlo analysis allows a direct evaluation of the uncertainties without the need to resort to ambiguous regression analyses and rules of combination of the uncertainties of demand and capacity based on the regression analysis results or other uncertainty estimation approaches.

1. Introduction

History, recent and past, reveals that tsunamis are among the most dangerous and destructive events. Geology aids in recognizing that there has been a periodical recurrence of tsunamis for several centuries. This justifies the efforts of the scientific community and global organizations in trying to understand tsunami hazard, vulnerability of constructions and population preparedness in such a way as to provide a probabilistic representation of the possible losses and to propose strategies for risk mitigation [1].

Deaths and destruction of tsunamis in the last decades give an idea that much has to be done. Refer for example to the tsunamis of the Colombian Pacific coast in 1906 and 1979, of Italy in 1908, of Japan in 1993, of Indonesia in 2004 and 2018, of Samoa in 2009, of Chile in 2010, of Japan in 2011 [2–9]. The latter event was particularly remarkable because of the nuclear disaster after the Fukushima power plant was inundated by the tsunami waves. In Fig. 1, the effects of this tsunami on the city of Ishinomaki are shown providing a measure of the destructive power of this event. All of these tsunamis were caused by earthquakes, however, underwater landslides or volcanic eruptions may cause destructive tsunamis as well. An example is the Alaska tsunami in 1958 [10].

Historically, the Mediterranean coasts were hit by catastrophic tsunamis: for example in 365 A.D., an earthquake with epicentre close to Crete Island was followed by a tsunami that caused 50,000 deaths along the coasts of Egypt, Greece, Sicily and Palestine; in 1169, 20,000 deaths were counted along the coasts around Catania because of a tsunami; in 1693, a tsunami caused over 60,000 deaths in Italy and Greece; in 1783, about 2000 deaths were registered in the Sicilian coasts of Messina and Reggio Calabria; in the same coasts, in 1908, a tsunami caused waves up to 12 m high and 40,000 deaths.

Among the structures exhibiting high vulnerability to tsunamis, masonry and wood structures have been revealed to be the most critical. Lower vulnerability has been observed for reinforced concrete structures and steel structures [11].

Fragility curves are powerful tools for the prediction of the probability of collapse or damage to an action of assigned intensity. In this framework, the experience gained in the case of earthquakes is fundamental [12–16]. In the case of tsunamis, fragility curves can accurately depict the state of the coastal areas after a critical event. If used as a prediction tool, fragility curves in combination with the site hazard aid in defining appropriate policies for the mitigation of tsunami risks

* Correspondence to: University of Palermo, Viale delle Scienze, Palermo, Italy,.
E-mail address: liborio.cavaleri@unipa.it (L. Cavaleri).

https://doi.org/10.1016/j.istruc.2024.106421
Received 20 October 2023; Received in revised form 1 April 2024; Accepted 13 April 2024
Available online 25 April 2024

involving constructions. Large-scale analysis of coastal areas should be carried out to obtain analytical fragility curves for classes of constructions by quantitative methods. The introduction of simplifications in the quantitative approaches is consistent with the effort needed for a large-scale analysis.

The choice of the tsunami Intensity Measure (IM), as in the case of earthquakes, is an open issue. However, the most simple way to describe a tsunami intensity is through a physical parameter called *inundation depth* (h) [17–20], which is the height of the wave front impacting a construction. Alternatively, the flow velocity (u) or the momentum flux (hu^2), can be used, or again the Froude Number $F_r = u/\sqrt{gh}$ [21]. However, the use of these parameters is less usual because difficult to manage.

Empirical tsunami fragility curves, which are obtained by the observation of the scenario caused by a tsunami, are available in the literature for different types of buildings [22–25]. These curves are obtained by estimating, by a field survey, the cumulative damage probability exceedance and assuming a lognormal distribution of the damage probability. This approach needs to fix a measure of the uncertainties involved, which converge to a unique number that synthetically encloses the uncertainties associated with demand and the uncertainties connected to structural capacity. Analytical fragility curves have been proposed as a prediction tool for different types of constructions [17–19,26]. Recently, Ferrotto and Cavaleri [27] proposed an approach for masonry buildings in the Mediterranean area.

Both for empirical and analytical fragility curves, the definition of the parameter involving the uncertainties is crucial. A comparison between fragility curves having the same median value of the intensity (that is the value of the intensity to which a 50 % exceedance probability corresponds) but different standard deviation values is shown in Fig. 2. The standard deviation influences the slope of the curve, in particular, the increment of the slope corresponds to a reduction of the uncertainty parameters.

The assessment of the uncertainty is generally obtained as a combination of the demand uncertainties and the capacity uncertainties, after a regression analysis to define a correlation, on average, between intensity of the external action and structural response, as will be better clarified hereinafter. If the procedure for the fragility evaluation is based on a Monte Carlo simulation, this approach is not useful because increases the computational effort and the possibility of inconsistent results as will be discussed in the following sections, where the procedure proposed in [27] will be resorted for comparison highlighting each time the advantages of a Monte Carlo simulation.

2. Fragility distribution and uncertainties

As mentioned before, fragility curves are cumulative distribution functions that can express the probability of exceedance of a building

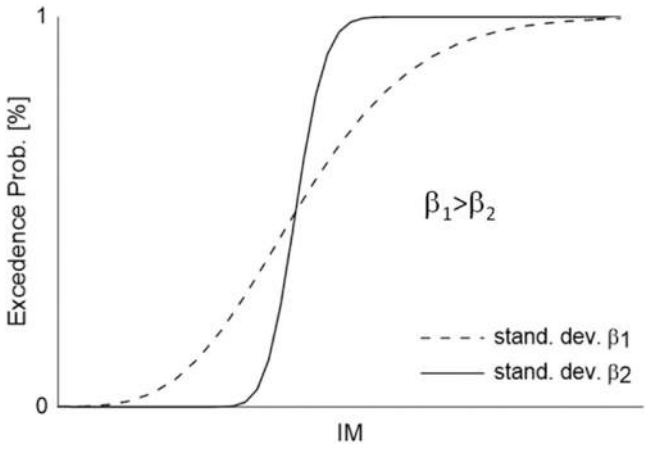

Fig. 2. Fragility curves characterized by the same IM median but different standard deviations.

Damage State (DS) over a range of values of an input intensity.

The assumption of lognormal distribution of the input intensities causing the before-mentioned damage state is the most successful. Under this assumption the conditional probability density function p is

$$p(DS|IM) = f(IM) = \frac{1}{IM \cdot \beta \cdot \sqrt{2\pi}} \cdot \exp\left(-\frac{(\ln IM - \mu)^2}{2 \cdot \beta^2} \right) \quad (1)$$

where μ and β are the mean and the standard deviation of the IM logarithmic values, respectively. A typical shape of the probability density function in question is shown in Fig. 3, evidencing that the random IM

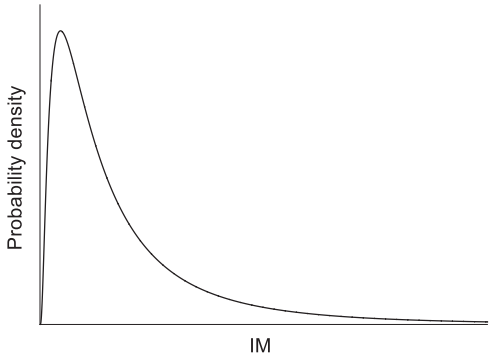

Fig. 3. Shape of a conditional probability density function in the case of lognormal distribution.

Fig. 1. Effect of tsunami on the city of Ishinomaki (Japan) in 2011.

value is defined among the positive real numbers consistently with the physical meaning of IM itself which cannot assume negative values.

The cumulative probability distribution function (cdf) associated with the probability density function (1) is obtained as

$$F(IM) = \int_0^{IM} p(DS|z)dz = \int_0^{IM} \frac{1}{z\cdot\beta\cdot\sqrt{2\pi}}\cdot\exp\left(-\frac{(\ln z-\mu)^2}{2\cdot\beta^2}\right)dz \quad (2)$$

It is simply proved that Eq. (2) can be expressed as

$$F(IM) = \frac{1}{2}\cdot\left[1+\mathrm{erf}\left(\frac{\ln IM-\mu}{\beta\sqrt{2}}\right)\right] \quad (3)$$

where $\mathrm{erf}(\cdot)$ is the error function, that is

$$\mathrm{erf}\left(\frac{\ln IM-\mu}{\beta\sqrt{2}}\right) = \frac{2}{\sqrt{\pi}}\int_0^{\frac{\ln IM-\mu}{\beta\sqrt{2}}} e^{-t^2}dt \quad (4)$$

Because the probability density function (pdf) is defined for positive values of IM, consistently with the meaning of IM itself, this pdf is more appropriate than the Gaussian distribution that is defined in the range [-∞ , + ∞]. However, the analytical advantages of a Gaussian distribution are maintained because of the dependence of the lognormal distribution statistics on only two parameters, mean μ and standard deviation β of the logarithms of IM (that is generally the inundation depth as discussed above).

As regards the value to be assigned to the parameter β representing the uncertainties, several approaches have been proposed in the literature, therefore a standard methodology has not yet been available. Karafagka et al. [18] considered statistically independent uncertainties for both demand and capacity, setting the uncertainties based on HAZUS-MH guidelines [28]. To this point, the overall standard deviation β is calculated as the square root of the sum of squares of the uncertainties assigned to demand (β_D) and capacity (β_C), that is

$$\beta = \sqrt{\beta_C^2+\beta_D^2}\,. \quad (5)$$

Medina et al. [19] tried to evaluate uncertainties by combining a Monte Carlo generation of the parameters for tsunami forces and r.c. frame building materials, but in that case, the effort for the non-linear analyses used for the comparison between capacity and demand, limited the capacity uncertainties to the characteristics of the materials, assuming as deterministic the building geometry. However, taking into account the variability in the geometry is basic for predictions in large areas.

In [27], a similar approach was adopted based on a Monte Carlo simulation including, among the random variables, the structural geometry, the mechanical characteristics of the material, the tsunami horizontal loads, the vertical external forces due to weight and service loads and the internal forces derived by the random combination of structural geometry and external forces. The combination of the uncertainties of capacity and demand (assumed statistically independent) by Eq. (5) is obtained after the statistical processing of the results. Preliminarily, a regression analysis for obtaining a correlation between inundation depth logarithms and structural internal forces (demand) due to tsunami actions is used. The regression curves provided the set of values of inundation depth logarithms strictly corresponding to the structural capacities backwards for the assessment of the inundation depth statistics. Finally, standard deviation of capacity and demand were combined in agreement to Eq, (5). This approach causes inevitably a loosing of information about the probabilistic variability of the inundation depth strictly depending on the regression analysis. Further, the independence, from the statistical point of view, of capacity and demand is a simplification whose reliability is not sure. In fact, the demand (the internal forces corresponding to the inundation depth) is strictly dependent on the structural geometry that affects the structural capacity.

The alternative is, once a random distribution for each involved random variable is fixed, to carry out a Monte Carlo simulation obtaining the parameter β, synthetizing the uncertainties of all the involved random variables. This is achieved directly by the statistical processing of the analysis results, without any further approximation or approximated assumption, using a backward strategy as described hereinafter. Therefore, the overall uncertainty β can be the result of the Monte Carlo analysis without any further approximated manipulation of the results as it will be better explained in the following sections.

3. Actions due to tsunami

Tsunami events induce various load effects on structures, as reported in FEMA P-646 [29] and ASCE/SEI 7–16 [30]. Loads caused by tsunami waves strictly depend on the inundation depth, that is the height of the water flow impacting a construction, and the flow velocity. Loads increase when the inundation depth and the flow velocity increase. The dynamic components of the loads are influenced by velocity and inundation depth while the static components are influenced by inundation depth only. In general, loads caused by tsunamis include hydrostatic and hydrodynamic components, water impact (impulsive component), debris impact, debris damming, buoyancy and uplift forces, water retention at elevated floors, and scouring effects [31–38] Since these forces do not occur simultaneously, the standard codes provide recommendations for combining them when applied on structures.

In this study, the evaluation of tsunami forces follows the approach proposed by FEMA P-646 [29], considering two main phases of loading. The first one is characterized by an impulsive force (F_i) and the second phase is characterized by a force obtained as the sum of the hydrostatic (F_h) and hydrodynamic (F_d) actions. These forces depend, in each case, on a specific inundation depth (h) and flow velocity (u). The hydrodynamic force (F_d), uniformly distributed, is evaluated depending on the angle - called α – between the flow direction and the front of the impacted building, the hydrostatic action has a classical triangular distribution with zero corresponding to the water flow upper surface. Further, the impulsive force (F_i), acting at the moment of the first wave impact and assumed for sake of simplicity with the same direction as the hydrodynamic component, is evaluated as 1.5 times the hydrodynamic component itself. No other forces are here considered to evaluate the response of buildings because of a real difficulty in their determination or because not decisive in the building damage. In conclusion, the resulting external forces for each horizontal meter of construction breadth impacted are evaluated as:

$$F_h = C_0\frac{1}{2}\rho g h^2; \qquad F_d = C_0\frac{1}{2}\rho C_D\left(h\cdot u^2\right)f(\alpha); \qquad F_i = 1.5F_d \quad (6)$$

where ρ is the density of the fluid, which includes sediments, and is assumed equal to 1100 kg/m^3 , g is the gravitational acceleration and C_D is the drag coefficient, measuring the resistance of an object in a fluid environment, $f(\alpha)$ depends on the direction of the water flow with respect to the impacted surface. It allows to calculate the component of the force orthogonal to the building surface, that is $f(\alpha)=\cos\alpha$ or $f(\alpha)=\sin\alpha$ depending on the side of the building considered). Further, C_0 takes into account the opening ratio of the impacted surface. Hence, $C_0 \leq 1$.

It is very difficult to know the maximum velocity associated with a fixed inundation depth h during a tsunami event. However, there is a convergence in stating that the Froude number (that is a parameter used to characterize the flow of fluids, hereinafter called F_R) has to be less than 2 according to Matsutomi and Okamoto [39] and Attary et al. [40], that is:

$$F_R = u\Big/\sqrt{gh} < 2 \quad (7)$$

Consistently with the superior limit, the value u_{max} fixed for the flow velocity is:

$$u_{max} = 2\sqrt{gh} \quad (8)$$

The limits for the flow velocity assigned in this way are consistent with the limits depending on the vertical run-up R and the ground elevation of the construction with respect to the mean level of the sea (here called z) [19]:

$$u_{max} = k\sqrt{2gR\left(1-\frac{z}{R}\right)}, k_{max} = 0.7 \quad (9)$$

$$\left(hu^2\right)_{max} = gR^2\left(0.125 - 0.235\frac{z}{R} + 0.11\left(\frac{z}{R}\right)^2\right) \quad (10)$$

However, in this study, the ground elevation of the construction has not been considered, therefore, for the limit of the flow velocity u, only Eq. (8) has been referred to.

4. The updated methodology for the definition of fragility curves

The procedure for the definition of fragility curves is synthetized in the flow chart in Fig. 4. It starts from the generation of tsunami events by the random generation of a set of flow velocities associated with a specific inundation depth and replicating the generation of u for different values of the inundation depth. In this way, hydrostatic, hydrodynamic and impulsive components can be calculated each time. These forces depend on the shape of the building impacted so a definitive calculation of them depends on the generation of the construction geometry.

Therefore, the h-u couples (inundation depth-flow velocity) are used for the evaluation of the hydrodynamic and impulsive forces that depend also on the breadth of the construction in the direction orthogonal to the flow. The next step is the evaluation of the internal forces to be compared with the capacity depending on the geometry but also on several random variables such as the material mechanical parameters, the orientation of the structural elements of the slabs affecting the level of vertical loads, the opening ratio and so on.

All the analyses carried out for an assigned value of h, after the random generation of all the variables involved, allow the recognition of the percentage of cases in which the limit state considered is overcome. This way, a direct construction of the fragility curve is possible containing the uncertainties of the demand and of the capacity, without any assumption of probabilistic independency of capacity and demand themselves.

In the previous version of the approach formulated for masonry constructions (Fig. 5), the uncertainties of capacity and demand are evaluated separately and then combined assuming that capacity and demand are independent random variables. To this aim, regression analyses of the logarithm of inundation depth – logarithm of Engineering Demand Parameters (EDP) pairs are performed. Once building structure models are generated, the capacities are calculated and used as input in the regression fitting curves to obtain the corresponding logarithms of h whose statistic processing provides the uncertainties of the capacity. Then, the uncertainties of the demand are calculated referring to the differences between the points of the regression curve and the ln$h$-EDP points generated for the Monte Carlo analysis (In Fig. 6, a regression fitting curve before mentioned is reported for a better explanation).

Finally, fragility curves are obtained by combining the log-standard deviations of the demand (β_D) and of the capacity (β_C) in agreement with Eq. (5). As can be observed, the past procedure is not linear and involves approximations not so necessary when the approach used is the Monte Carlo simulation.

In the following section, an application of the updated procedure to different classes of buildings is proposed evidencing the details, the effectiveness and the rigor of the new procedure itself.

5. Application details for some class of buildings

5.1. Structural modeling and capacity models

Two and three-storey residential regular masonry buildings are typical along the coasts of the Mediterranean Sea, as in the case of Sicily, North Africa, Greek islands and so on. In Fig. 7, aerial images of

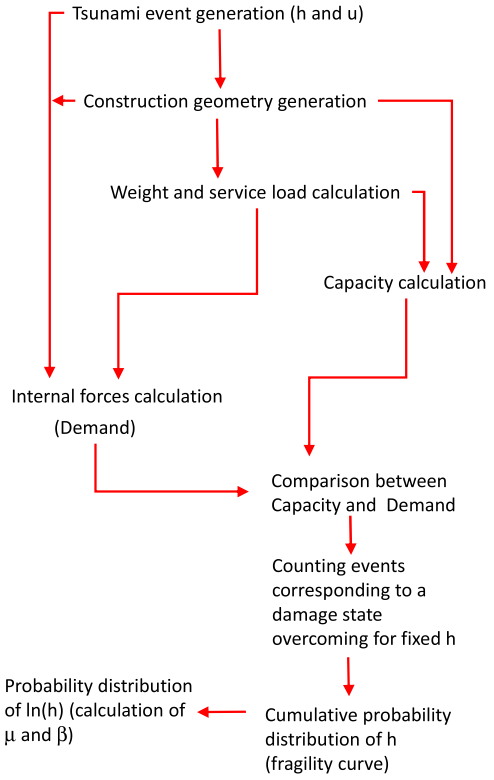

Fig. 4. Flow chart of the updated strategy for the assessment of tsunami fragility curves.

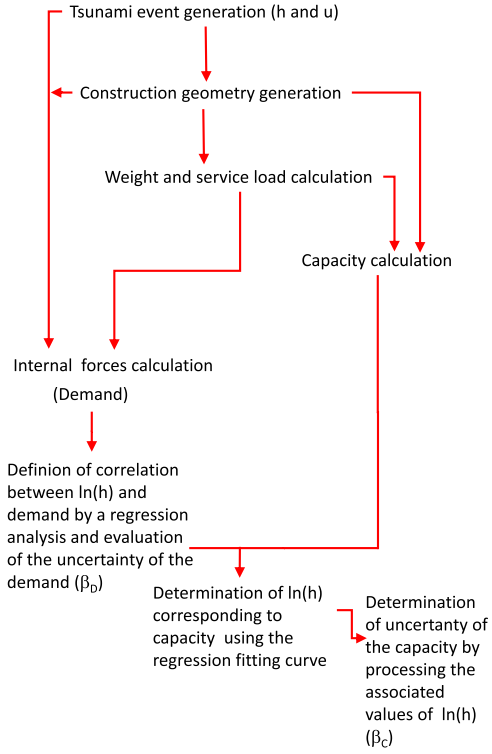

Fig. 5. Flow chart of the original previous strategy for the assessment of tsunami fragility curves.

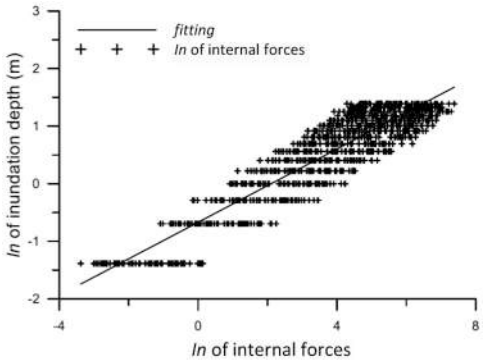

Fig. 6. Example of regression analysis of the $ln(h)$ – EDP pairs.

buildings in Sicily and Malta are shown. Such buildings will be the object of the following applications. In Fig. 8, a schematic plan of the buildings considered is shown where the dimensions of the walls and of the openings, as well as the position of the openings are considered random variables.

The behavior of masonry buildings subjected to tsunami loads has been identified through simplified local models, considering that the global collapse is identifiable with a local collapse as usual in the practical applications and suggested by different codes.

Therefore, a local analysis has been performed to recognize the structural collapse. In detail, the out-of-plane (OOP) response of walls directly impacted by the water flow is considered, as well as the in-plane (IP) response of walls, whose middle plane contains the water actions, that are not directly impacted by the water but to which wave action is transferred by walls directly impacted. In the case of OOP actions, vertical and horizontal bending are considered separately. In the case of IP action, bending and shear are both taken into account. In detail, Fig. 9 shows a wall impacted by a water flow and the schemes for the calculation of the demands in terms of horizontal and vertical bending. In the case of vertical bending, the masonry wall is modelled as a simply supported beam whose constraints correspond to the position of the slabs (Fig. 9-b), while, in the case of horizontal bending, the wall is modelled as a simply supported beam with constraints corresponding to the position of the bordering orthogonal walls (Fig. 9-c).

Fig. 10 shows a wall that, due to the water flow, is characterized by an in-plane loading. In this case, the demand is calculated by the translation and rotation equilibrium conditions using, as external actions, those applied on the influence area of the wall directly impacted by the water flow.

Thickness t and in-plane dimensions of the walls, including openings, are considered random variables, uniformly distributed, in a range consistent with the real cases. Also, mechanical masonry characteristics (compressive and shear strength) are random variables. Differently from the previous ones, and as usual in the practice codes, these are assumed

Fig. 7. Examples of masonry buildings along the Mediterranean coasts: a) and b) Syracuse, in Sicily, c) St. Paul bay, in Malta.

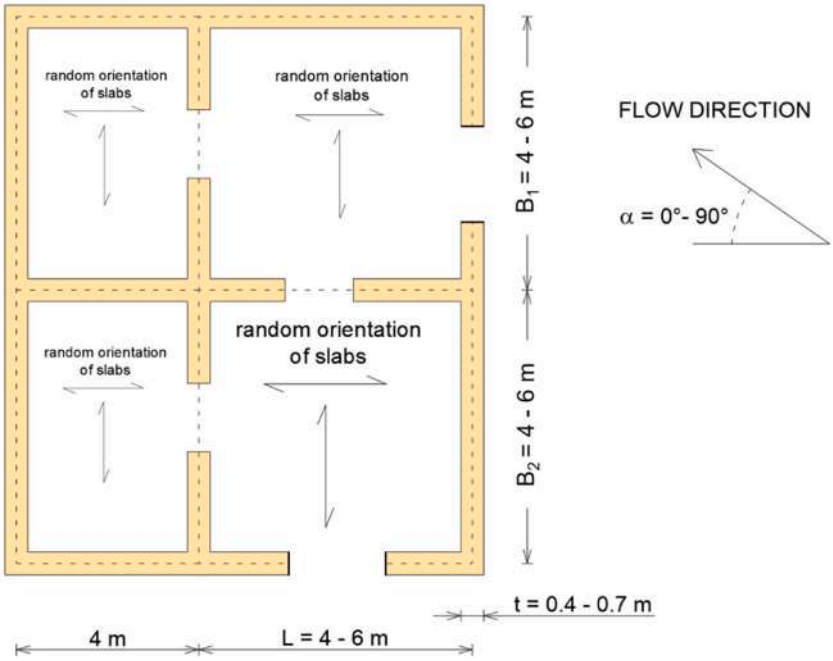

Fig. 8. Plan geometry model of the classes of masonry buildings analyzed.

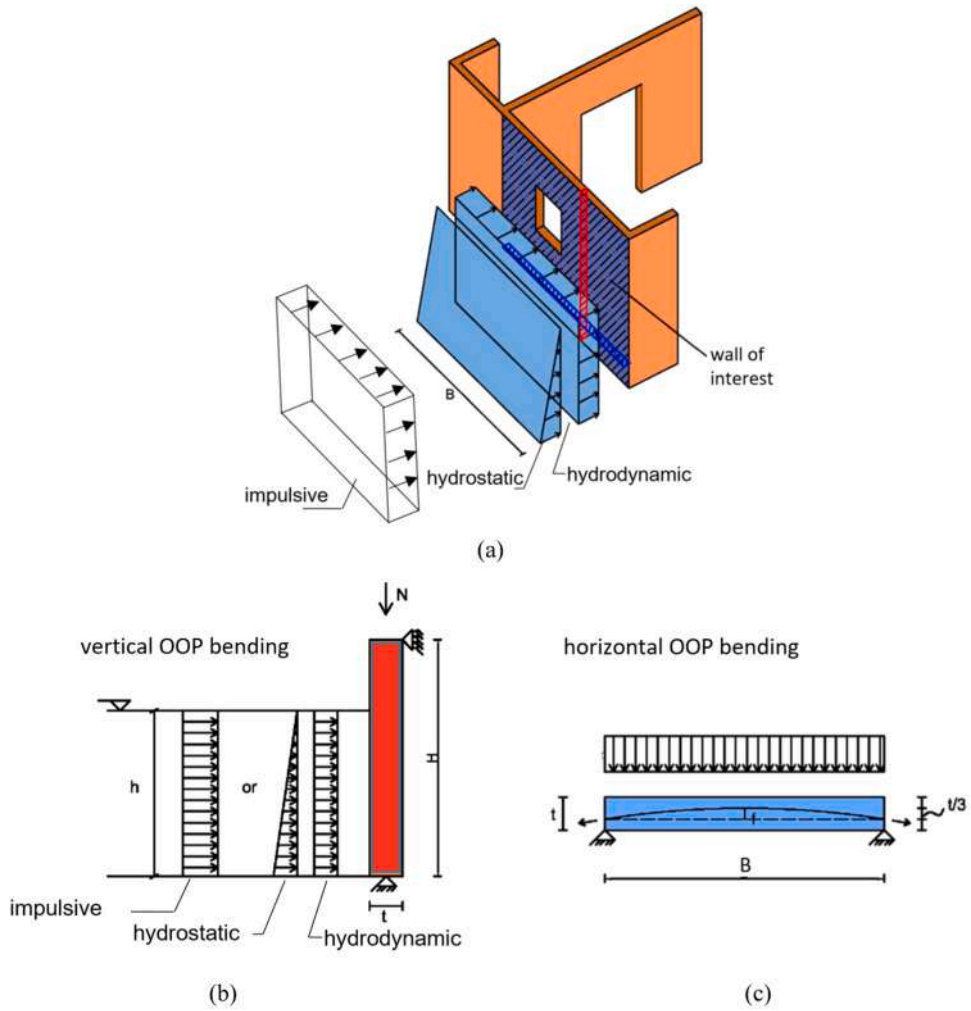

Fig. 9. OOP local model: a) three dimensional scheme, b) scheme for vertical bending, c) scheme for horizontal bending.

normally distributed.

5.1.1. Out-of-plane behavior

Internal forces (vertical and horizontal bending) are evaluated by applying the loads according to the schemes shown in Fig. 9. Vertical bending is evaluated by considering the distributed load on a beam having a cross-section equal to $B{\cdot}t$. While, the horizontal bending is obtained by calculating the action on a beam having cross-section $H{\cdot}t$, distributed on the breadth B of the wall.

The vertical bending capacity of the cross-sections is obtained according to the current Italian Building Code 2018 [41] by means of the following equation.

$$M_{\max,OOP_v} = \left(C_O{\cdot}t^2{\cdot}B{\cdot}\frac{\sigma_0}{2}\right)\left(1-\frac{\sigma_0}{0.85f_m}\right) \tag{11}$$

being σ_0 the mean compressive stress acting on the cross-section (that is $\sigma_0 = N/(B{\cdot}t)$), f_m the masonry compressive strength, t the wall thickness, C_O the opening coefficient (that is (B-w_0)/B being w_0 the sum of the horizontal lengths of the openings in the wall considered) and B the breadth of the masonry wall subjected to the tsunami wave.

The horizontal out-of-plane bending capacity is evaluated by considering the arch effect of the masonry walls. The mechanism is exhibited by the expulsion of material from the top area of the wall and the detachment of wedge-shaped bodies accompanied by the formation of oblique and vertical plastic hinges. It is the particular case in which the activation of the kinematic mechanism is due to the crushing of the masonry at the plastic hinges, then the capacity is

$$M_{\max,OOP_h} = f_m{\cdot}C_O{\cdot}H{\cdot}\frac{t}{2}{\cdot}f; \quad f = \frac{t}{3} \tag{12}$$

In Eq. (12), H is the height of the masonry wall, and f defines the position of the resultant of the internal forces at the ending cross-sections (Fig. 9-c). Note that, due to the assumption of a certain percentage of openings in the walls, the resisting area has been reduced by applying the opening coefficient ($C_O \leq 1$) to the bending moment resulting from the capacity models (11) and (12). Consider that the opening coefficient for the vertical bending capacity is not necessarily equal to the opening coefficient for the horizontal bending capacity. Also, the opening coefficient used in the evaluation of the tsunami forces may be different depending on the inundation depth. If the latter is lower than the height H of the wall, then the upper surface of the water may cross an opening determining a different opening ratio (for the scope of the calculation of the action caused by the water flow) with respect to the calculation of the effective wall capacity.

5.1.2. In-plane behavior

The in-plane bending moment and shear are obtained according to the scheme shown in Fig. 10. The wall in question is not directly impacted by the water flow but the forces are transferred by the close walls directly impacted by the water flow in the OOP direction. Therefore, the external forces are evaluated considering the resultant on the effective surface of the walls directly impacted by the water. The effective surface before mentioned is obtained considering the scheme

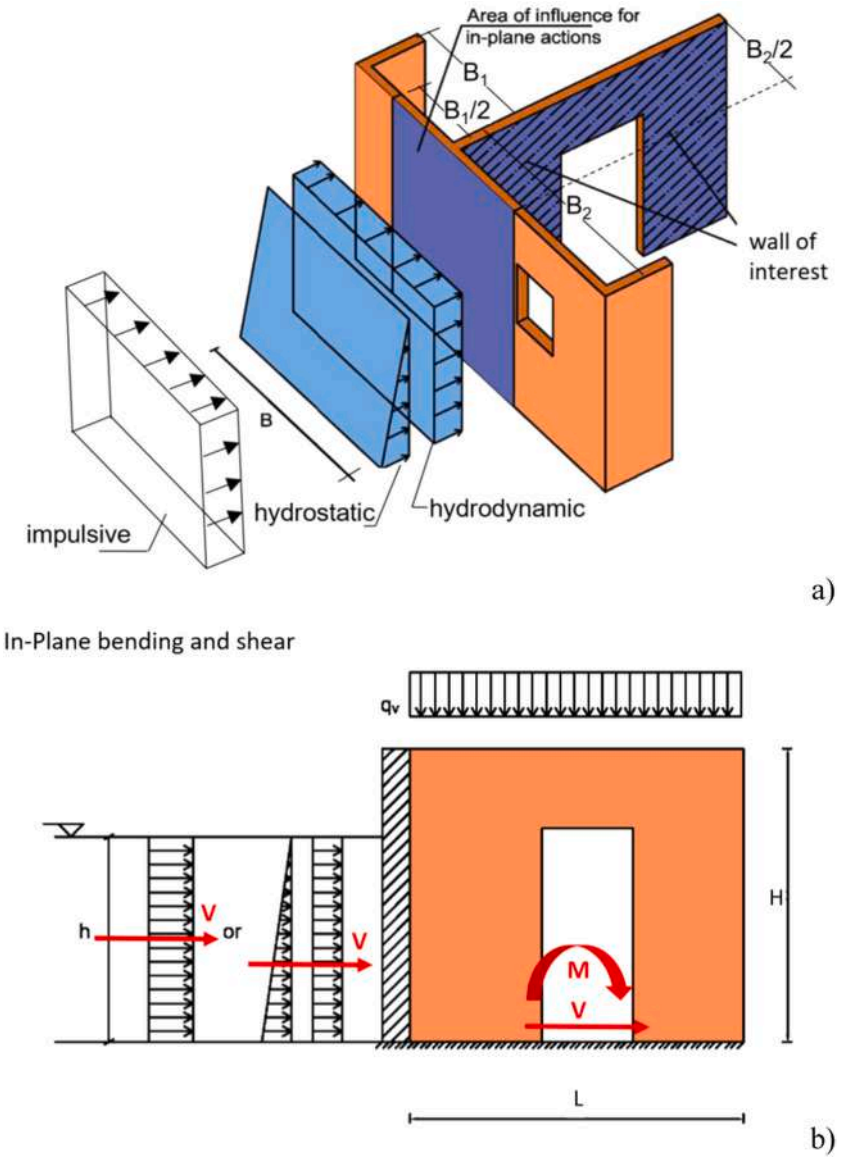

Fig. 10. IP local model: a) three dimensional scheme, b) scheme for bending and shear.

proposed in Fig. 10 by which it is possible to evaluate the in-plane shear and the in-plane bending moment. Differently from the case of seismic analysis where the forces are applied at floor level, in the case of tsunami forces, the application point of the tsunami loads depends on the inundation depth and the distribution of the forces may be not properly depending only on the stiffness of the walls. If the wall in question has an opening, the majority of shear forces are absorbed by the part of the wall closer to the water flow. However, in the case of a good connection with the slabs and in the case of rigid slabs, the distribution may be very similar to the seismic case. This is the hypothesis here assumed.

As regards the capacity, the Italian Building Codes [41,42] for the moment and the shear have been referred to and the bending and shear capacities have been calculated in a simplified way as follows:

$$M_{\max\,,\,IP_v} = \left((C_O \cdot L)^2 \cdot t \cdot \frac{\sigma_0}{2}\right)\left(1 - \frac{\sigma_0}{0.85 f_m}\right) \tag{13}$$

$$V_t = C_O \cdot L \cdot t \cdot \frac{1.5\,\tau_0}{b}\sqrt{1 + \frac{\sigma_0}{1.5\,\tau_0}} \tag{14}$$

where the coefficient C_0 has been inserted to take into account the capacity reduction due to openings. In detail, Eq. (13) represents the bending moment capacity for a given axial load $\sigma_0 = N/(L \cdot t) = q_v/t$ (see Fig. 10 for a better comprehension of the meaning of the symbols). Eq. (14) expresses the shear capacity related to the diagonal shear failure provided by the Turnsek-Cacovic failure criterion, in which τ_0 is the average tangential strength. In general, technical Codes provide a specific range of τ_0 for each masonry typology.

5.2. Damage state

For the analytical evaluation of tsunami fragility, there are different approaches available in the literature that consider different indexes for global and local damage [17–20]. It is worth noting that these approaches refer generally to the analytical evaluation of tsunami fragility of reinforced concrete structures. Approaches are available for masonry building empirical fragility evaluation as those proposed by Suppasri et al. [22,23], associating the building conditions at the end of the tsunami inundation with specific indexes depending on the damage states encountered (non-structural damage, slight damage, medium damage, extensive damage, collapse or washed away). However, the definition of proper damage states for analytical fragility evaluation is a real challenge because it is not easy to relate for sure the level of damage

observed in a real case to the variation of a mechanical parameter observed by an analysis, especially in the case of nonstructural damage. Conversely, the analytical recognition of the collapse state is consolidated.

In this application, the collapse is associated with the reaching of the capacity of the members evaluated by a local approach. For the scope of this study, that is to show how to obtain uncertainties in the definition of fragility curves, no other damage states will be considered, being however the here discussed procedure consistent with the possibility of considering any other type of damage state.

5.3. Distribution of the random variables involved in the Monte Carlo simulation

The methodology based on Monte Carlo simulations, consolidated in the field of seismic response [43,44], involves the generation of the structural geometry, the mechanical characteristics of materials and the parameters that characterize the tsunami events. Among the parameters for the geometry, the orientation of the structure of the slab is included affecting the level of the vertical forces on the walls and thus affecting their capacity. Here, the cases of two-storey and three-storey buildings are separately considered. Further, each case is split into two cases characterized by different probabilistic mechanical characteristics of the masonry. Each random variable is generated within specific ranges, as reported in Table 1, in accordance with the assigned probabilistic distribution. In particular, a Gaussian distribution is assumed for the material strengths, while a uniform distribution for the other variables in an appropriate way because of the characteristics of the variables considered [19]. The standard deviation of the Gaussian distribution of the strengths here assigned (accepted by some current standard codes, e.g. [41]) guarantees that the tails of the pdf go rapidly to zero in such a way Gaussian pdf does not provide a probability for not significative values (negative values or values close to zero).

In the case of uniform distribution, the variable range is given, while in the case of normal distribution, mean and standard deviation are assigned.

As regards to the mechanical characteristics of the masonry, the Gaussian distribution may contemplate negative values that are excluded during the procedure. However, as it can be observed by the distribution of the masonry strengths (Fig. 11), the likelihood of generating values lower than zero is really low, quickly converging the tails of the pdf to zero.

As mentioned before, for the masonry mechanical properties, two distinct strength classes (referred to as “case 1″ and “case 2″) have been assigned (this assignment was aimed also to test the influence of these mechanical properties on the fragility). Mean and standard deviation values for compressive (f_m) and shear strength (τ_0) are fixed referring to the range provided by the Italian Building Code [41], which reasonably may be extended out of the Italian borders.

Table 1
Probabilistic characteristics of the random variables.

	random variable	range	mean	standard deviation	distribution
Materials	f_m (case 1)	-	2.3 MPa	0.26 MPa	Gaussian
	f_m (case 2)	-	3.4 MPa	0.26 MPa	
	τ_0 (case 1)	-	0.054 MPa	0.007 MPa	
	τ_0 (case 2)	-	0.085 MPa	0.007 MPa	
Geometry	B_1	4-6 m	-	-	uniform
	B_2	4-6 m	-	-	
	L	4-6 m	-	-	
	t	0.4-0.7 m	-	-	
	C_0	0.5 – 1.0	-	-	
	H	3 – 4 m	-	-	
	slab structure orientation	0° or 90°	-	-	
Tsunami load	u	0-u_{max}	-	-	uniform
	α	0° – 90°	-	-	

The geometry of buildings is generated based on the scheme in Fig. 8. Once, the direction of the tsunami wave is generated, the walls along the two building sides impacted by the wave are checked. The dimensions B_1, B_2, L, t, H and the opening coefficient C_O are generated in specific ranges of values (Table 1), consistently with the real cases. Additionally, the random orientation of the slab structures is assumed because strictly connected to the capacity of the walls. In fact, the mean level of the vertical stress σ_0 on the walls depends on the orientation in question, changing the outcome of Eqs. 11, 13, 14. A total number of 1000 different structural geometry models were generated and combined with the tsunami actions resulting by the generation of 3000 values of the velocity u for each value of inundation depth h. The levels of inundation depths in the range of 0.2 m – 4 m were investigated with a step of 0.1 m. Hence, 39 different levels of the inundation depth h were considered being the i-th level h_i given by

$$h_i = 0.2 + (i-1)\cdot 0.1 \tag{15}$$

Finally, each geometry model was loaded by different 39 × 3000 tsunami events, each of them characterized by a pair h-u. In the following Fig. 12 the distribution of the generated geometric parameters (1000 buildings for each class were generated).

Then, random values for the flow velocity u and the angle α defining the direction of the tsunami flow with respect to the structure orientation (refer to Fig. 8 to know the direction corresponding to the zero value) are generated, with the assumption of a uniform distribution. Fig. 13 shows the values of the flow velocity u generated for each value of the inundation depth h and the corresponding range consistently with the limits fixed by Eq. (8).

As before mentioned, the process involved the generation of 3000 values of velocity for each inundation depth resulting in 3000 × 39 tsunami scenarios. Considering that 1000 buildings were generated for each class, it resulted in N = 3000 × 1000 × 39 distinct analyses for each class, each of them including two load combinations (impulsive action on one hand and hydrostatic + hydrodynamic actions on the other hand). This strategy really guarantees the random characteristics of the input, which are basic for the probabilistic characterization of the structural behavior as often pointed out in the literature (e.g. [45]).

5.4. Monte Carlo simulation and distribution of inundation depth at the collapse

Therefore, Monte Carlo analysis included N = 3000 × 1000 × 39 analyses for each class of buildings considered (2 storeys – lower masonry strength (case 1); 2 storeys - higher masonry strength (case 2); 3 storeys - lower masonry strength (case 1); 3 storeys higher masonry strength (case 2)), each time giving a value of the collapse capacity to be compared with the demand.

It is necessary to point out that the Monte Carlo simulation here discussed disregards some sources of uncertainty because, for example, of the use of deterministic models of the capacity (Eqs. 11–14), of the deterministic assumption of the boundary constraints which characterize the walls out-of-plane loaded (Fig. 9) from which the demand depends and of some others assumptions. This fact is normal in a Monte Carlo simulation because generally some variables are assumed as deterministic and some others probabilistic. However, this may cause a loosing in the reliability of the probabilistic characteristics of the results. It occurs each time the deterministic assumptions in a Monte Carlo analysis do not find the true characteristics. In the cases here discussed, the deterministic assumptions involving capacity and demand are consistent with a behaviour that on average masonry walls are able conservatively to exhibit and, for this reason, these assumptions have been adopted. However, an enlargement of the list of the random variables can be worthy to be considered being the proposed procedure

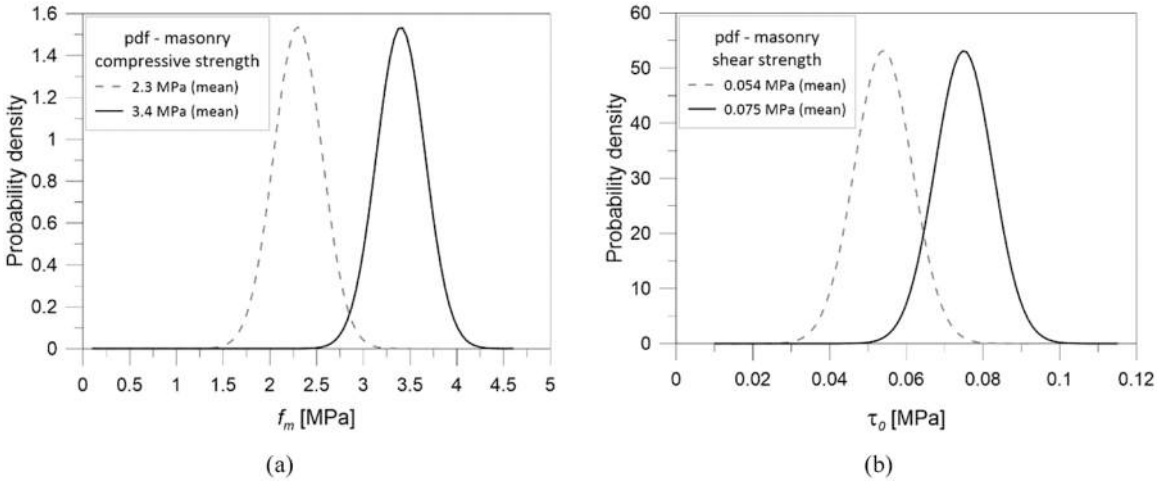

Fig. 11. Probability density functions of the compressive and shear masonry strengths: (a) case 1, (b) case 2.

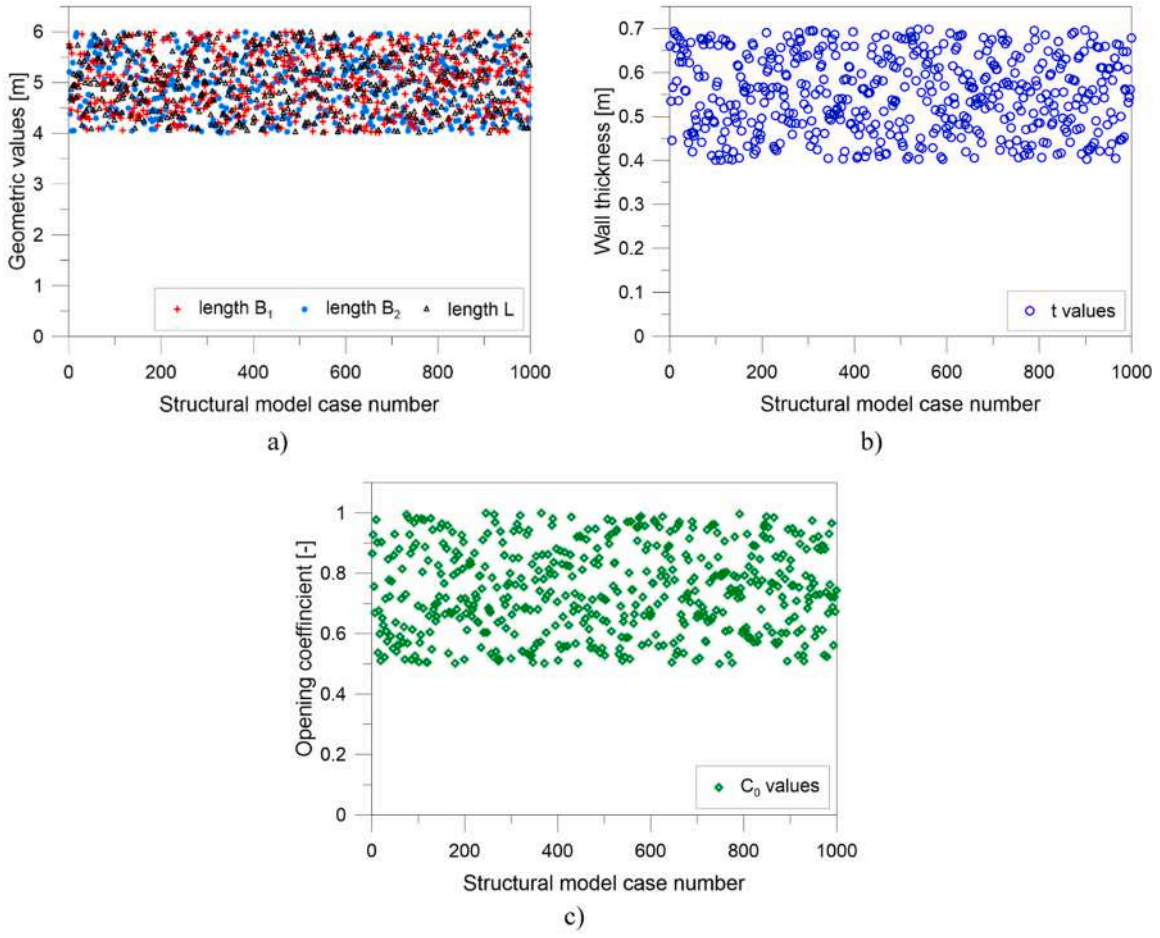

Fig. 12. Values generated for the geometric characteristics of buildings: a) length of walls (B_1, B_2 and L), b) thickness of walls (t), c) opening coefficient (C_0).

simply improvable to manage a higher number of them.

Both for the generation of the cases to be analyzed and for the analyses, the Python programming language [46] was used, importing Python libraries into the open-source PyCharm software. In detail, the capacity of each external and internal wall was calculated by using Eq.s 11–14 which allowed the assessment of out-of-plane and in-plane collapse forces for each structural model generated. In Figs. 14 and 15, the distribution of the capacities is inserted. It is evident that the level of the vertical loads (depending on the number of floors) influences the capacity in terms of vertical bending, caused by OOP action, more than the mechanical characteristics of the material. The influence of the latter seems negligible and this is consistent with the capacity model (11). It is similar for shear and in-plane bending (model (13) and model (14)) but not for the OOP horizontal bending because in that case there is no dependence of the capacity on the vertical load (see the model (12)). It is interesting because it reveals a dependence of a building's

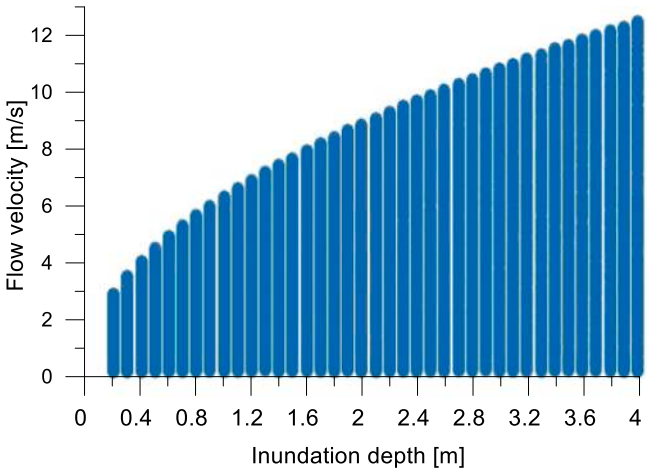

Fig. 13. Flow velocity values generated for each inundation depth.

vulnerability on its height that is worthy to be further deepened.

For each tsunami action, the ratio between structural capacity and tsunami demand (in terms of internal bending moments and shear) was calculated and during the iterations whenever the ratio was less than 1 the corresponding value of h was stored.

A count vector was created to count all the times that a specific inundation depth h caused the collapse damage state in agreement with the collapse mechanisms considered (OOP vertical bending, OOP horizontal bending, IP bending, IP shear). Subsequently, the count vector was normalized with respect to the total number N of cases analyzed (3000 ×1000 ×39) and the fragility points F(h_i) were obtained. In this stage, the value of the inundation depth causing the collapse of 50 % of the cases analyzed ($h_{50\%}$ - median value of the inundation depths of collapse) was identified and the logarithm of this value, representing the average of the logarithms of h, was also computed, that is

$$\mu = \log(h_{50\%}) \tag{16}$$

In order to evaluate the uncertainties (namely the standard deviation of the values of the inundation depths h associated with the incipient collapse) a backward procedure was used. First, the probability distribution of h was calculated starting from the fragility results. In details, the number of outcomes N_{h_i} for h=h_i was obtained as

$$N_{h_i} = \overline{N}_{h_i} - \overline{N}_{h_{i-1}} \tag{17}$$

where $\overline{N}_{h_i}$, that is the number of cases exceeding the collapse state at an inundation depth h_i, is obtained by multiplying the value of the fragility curve corresponding to h_i itself [$F(h_i)$] by the total number of cases N of the Monte Carlo simulation, namely:

$$\overline{N}_{h_i} = F(h_i) \cdot N \tag{18}$$

To this point, it was possible to calculate the standard deviation β of the logarithms of h as

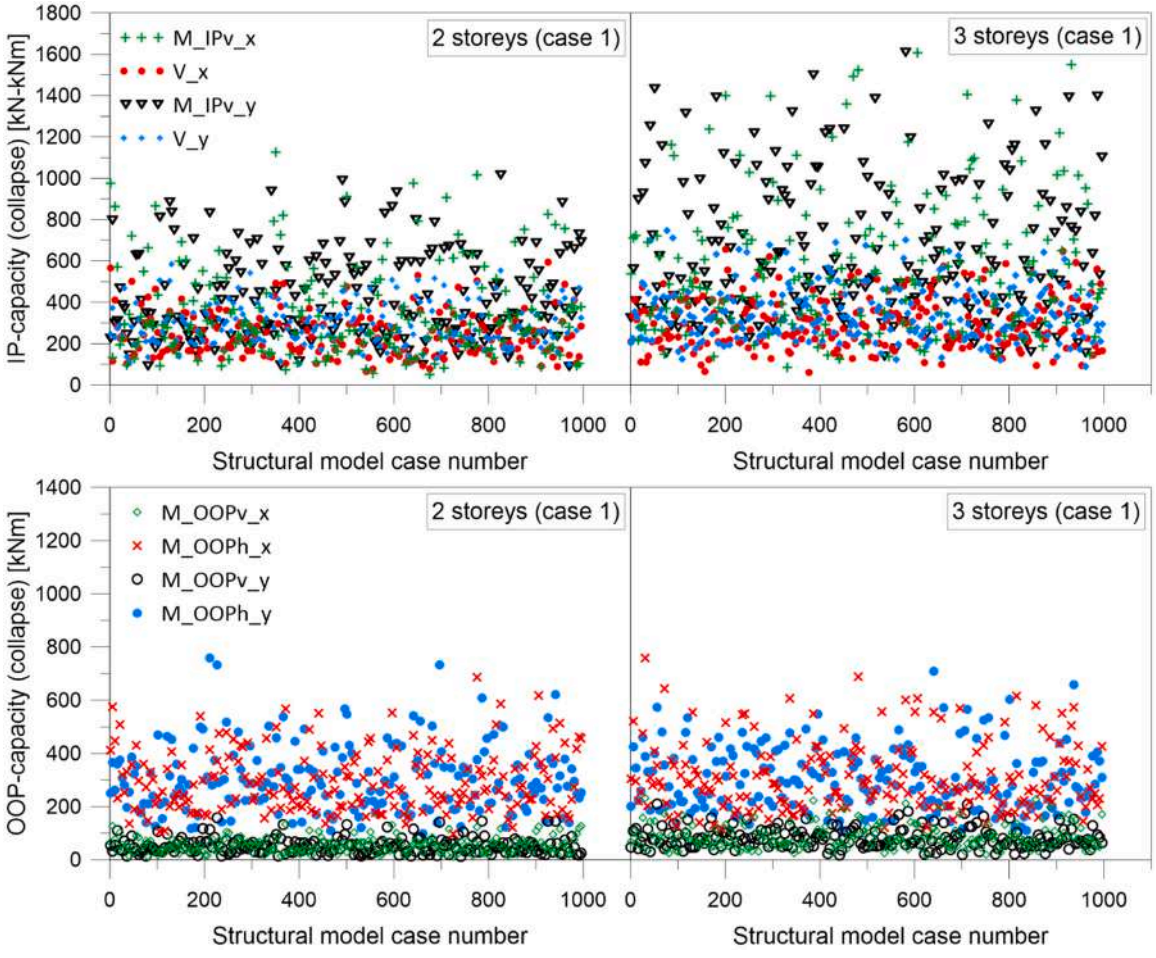

Fig. 14. Distribution of the capacities: case 1 (lower masonry strengths).

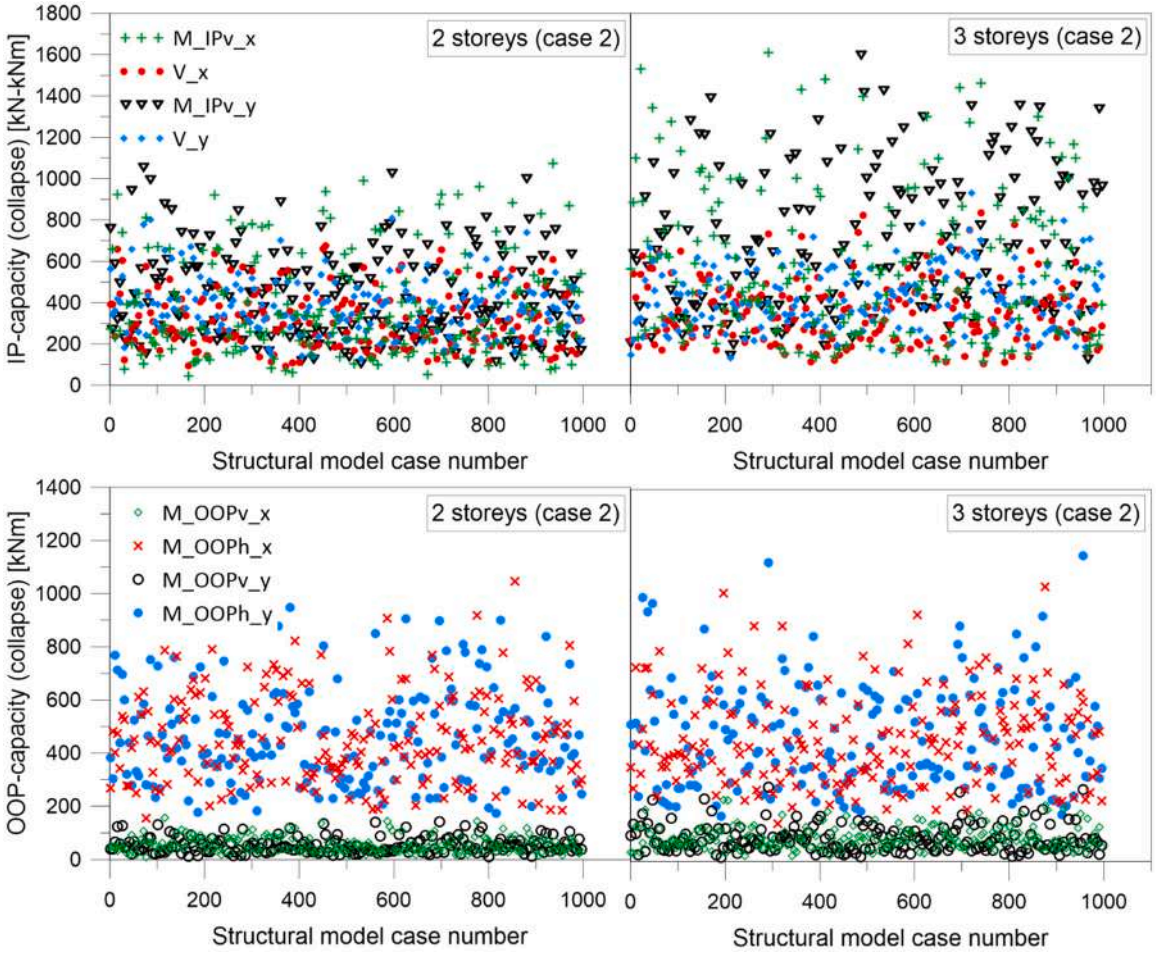

Fig. 15. Distribution of the capacities: case 2 (higher masonry strengths).

$$\beta = \sqrt{E\left[(\log h)^2\right] - E[(\log h)]^2} = \sqrt{\frac{\sum_{i=1}^{39} N_{h_i} (\log h_i)^2}{N} - \left(\frac{\sum_{i=1}^{39} N_{h_i} (\log h_i)}{N}\right)^2} \tag{19}$$

where $E[\cdot]$ is the average operator. It is worth observing that, the value of the standard deviation obtained encloses the uncertainties of the random variable involved (geometrical, mechanical and about the input) giving an overall representation in connection to the definition of the fragility curves. The approach used does not request the assumption of the independence of the capacity and the demand uncertainties and the use of Eq. (5), which does not reflect the real correlation between the random variables involved. In fact, the internal forces (demand) depend on the input and on the geometrical characteristics of a building. The latter contributes to defining the capacity. This makes more than one doubt arise about the hypothesis of probabilistic independence of capacity and demand.

The discrete conditional probability density distribution of the collapse obtained by the analyses has been compared with the lognormal pdf given by Eq. (1) once the average (μ) and the standard deviation (β) of the logarithms of h have been obtained by the results of the Monte Carlo simulation. In this connection, Fig. 16, in which the four classes of building analyzed, i.e. 2 storeys – case 1, 3 storeys – case 1, 2 storeys – case 2 and 3 storeys – case 2, gives evidence of the appropriateness of this type of probabilistic distribution and the capability of Eq. (1) to give a probabilistic representation of the number of incipient collapses associated to a certain value of the inundation depth.

In Fig. 16, the values of the mean of the logarithms of h (that is μ) and the standard deviation of the logarithms of h (that is β) are explicitly indicated. Further, the median (μ*) and the standard deviation (β*) of the inundation depth h are also included. From the results, it can be observed that the number of storeys causes an increase in the uncertainties higher than the variation of the mechanical characteristics of the masonry. This is due to the key role of the vertical loads in the capacity of the internal and external walls traducing in a different level of σ_0 in Eq.s 11, 13, 14. The increase in the number of storeys causes an increase in the range of σ_0 depending on the orientation of the slab structure. However, both increases in the number of storeys and masonry strengths cause an increase in the median value of the inundation depth, that is the value corresponding to a probability of collapse exceedance of 50 %. It is worth noting that the increase of the median value is relatively modest with respect to the masonry strength and becomes more pronounced as the number of storeys increases.

If the geometry is assumed as deterministic (this is the approach followed in [19]) leaving as random the material strengths and the inundation depth–flow velocity pairs, one observes, as expected, a reduction of the overall uncertainty. However, the lognormal distribution of the conditional probability density of collapse may be not appropriate as is shown in the next Fig. 17. In the latter case, a two storeys building is assumed as deterministic with intermediate masonry strengths compared to case 1 and case 2, previously considered. As it is clear, there is a level of inundation depth that causes the collapse of the structure in any case because of the hydrostatic action, which is independent of the flow velocity. This causes a sudden drop in the conditional probability density of collapse that makes the analytical curve of

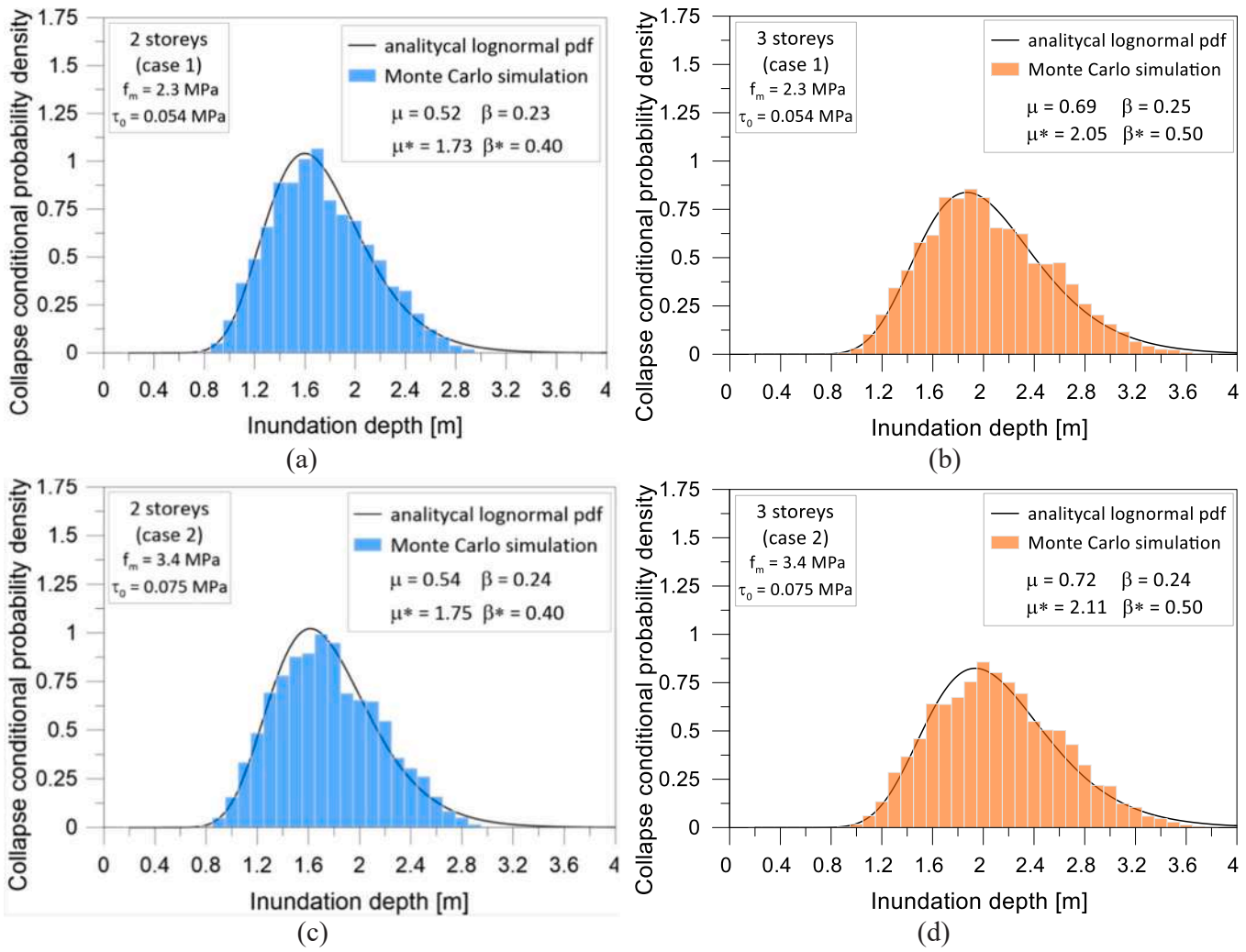

Fig. 16. Conditional probability density of collapse: a) 2 storeys - case 1; b) 3 storeys - case 1; c) 2 storeys - case 2; d) 3 storeys - case 2.

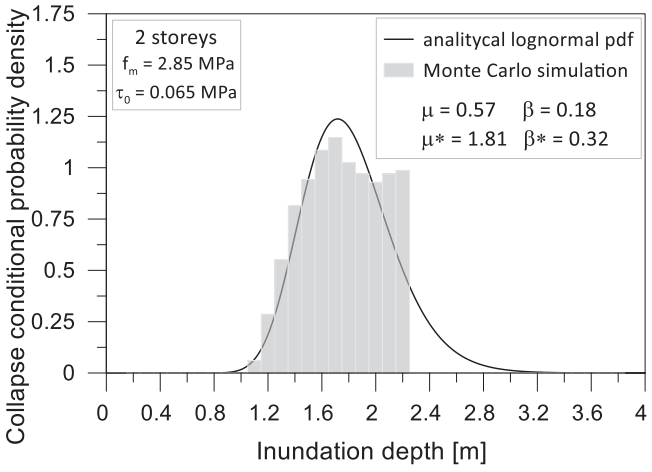

Fig. 17. Conditional probability density of collapse in the case of deterministic geometry.

the lognormal distribution move away from the results of the Monte Carlo analysis. This has a consequence on the fragility reliability, as it will be shown in the next section.

5.5. Fragilities

The results of the Monte Carlo simulations discussed in the previous section in terms of mean and standard deviation of the logarithms of the inundation depths associated with the collapse are used for the construction of the analytical fragility curves, the latter depending on these two parameters as widely discussed before. A comparison of the fragility points at the collapse derived by Monte Carlo simulation and the lognormal analytical distribution is included in Fig. 18 for the four distinct building typologies (2 storeys – case 1, 3 storeys – case 1, 2 storeys – case 2 and 3 storeys – case 2) considered. The comparison shows a good agreement between the model assumed for the probability distribution and the Monte Carlo simulation. It is worth noting that the median values of inundation depth corresponding to the collapse damage state were determined to be 1.73 m, 2.05 m, 1.75 m and 2.11 m for 2 storeys buildings – case 1, 3 storeys buildings – case 1, 2 storeys buildings – case 2 and 3 storeys buildings – case 2, respectively. The increase was much more evident in the case of a higher number of storeys which meanly determines an increase of the vertical loads on the walls improving the capacity, as before mentioned. The improvement of the mechanical characteristics of masonry (compressive and shear strengths) had a minor or almost negligible role in agreement with the bending and shear capacity models used. All this is clear from Figs. 19 and 20 where a comparison in terms of fragility is done in the case of different numbers of stories and in the case of different mechanical characteristics of the material.

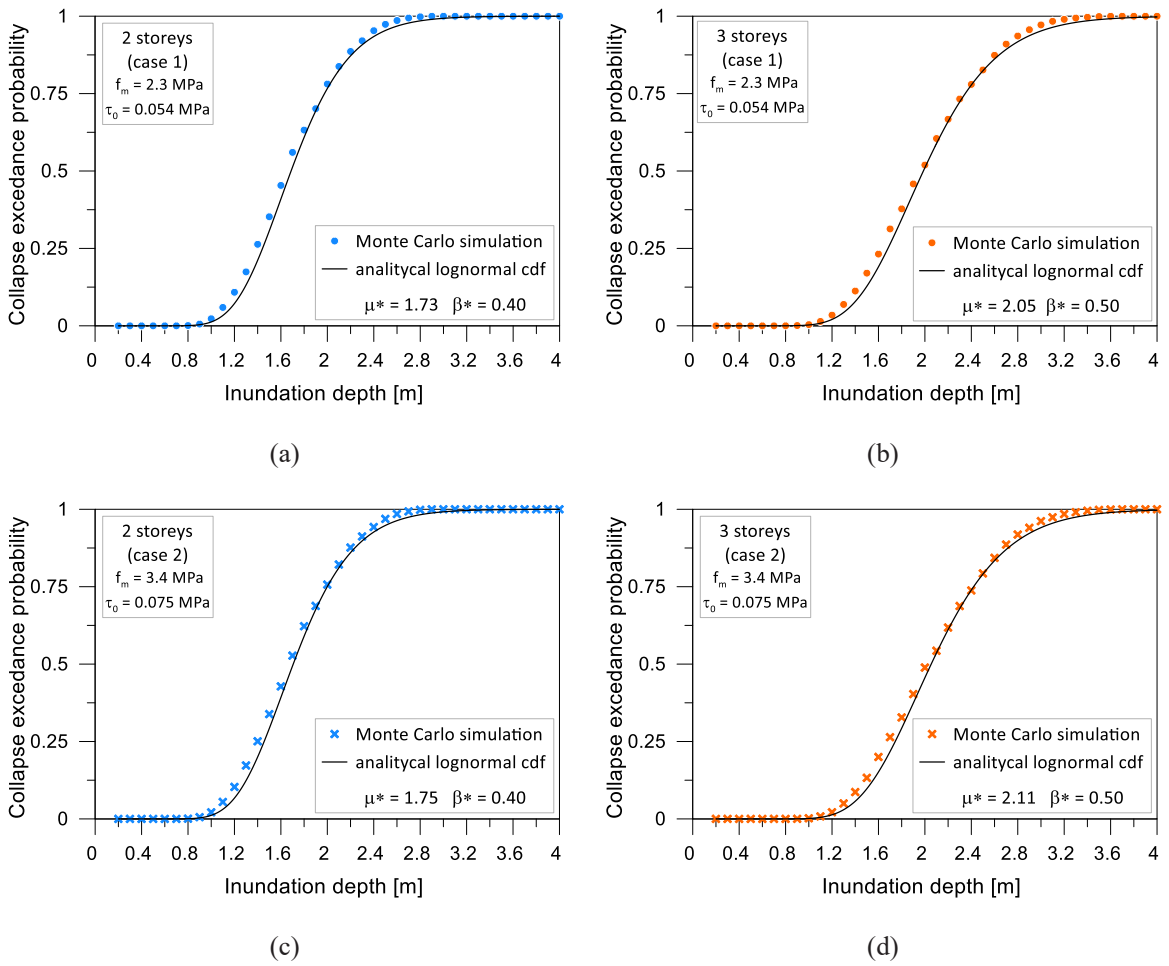

Fig. 18. Collapse exceedance probability: a) 2 storeys - case 1; b) 3 storeys - case 1; c) 2 storeys - case 2; d) 3 storeys - case 2.

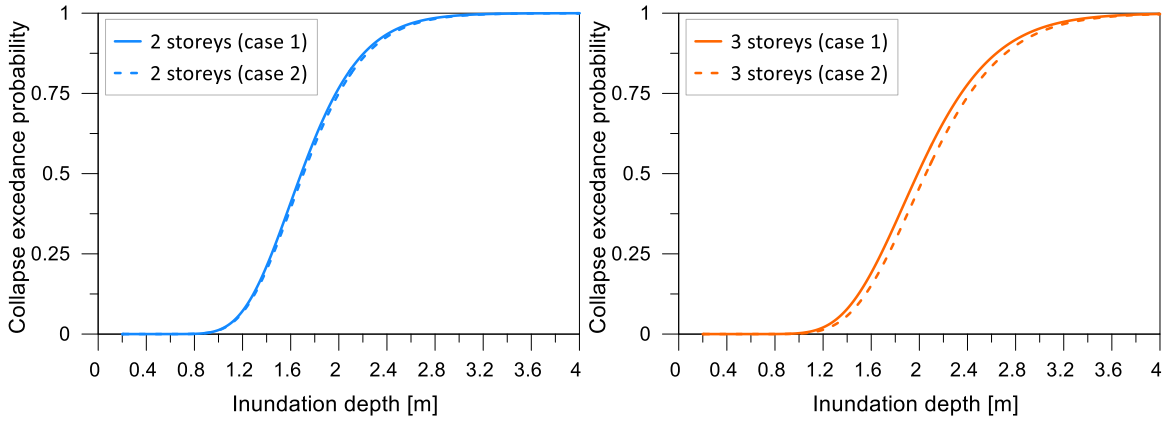

Fig. 19. Analytical collapse exceedance probability: a) comparison between 2 storeys buildings characterized by different strengths of masonry (case 1: lower; case 2: higher); b) comparison between 3 storeys buildings characterized by different strengths of masonry (case 1: lower; case 2: higher).

Figs. 19 and 20 really show that the higher influence on the fragility is given by the level of the vertical loads due to the number of storeys. In fact, the increment of vertical load causes an increasing of the wall capacity.

For the sake of completeness, the fragility points obtained in the case of deterministic geometry are inserted in the figure below, evidencing an underestimation of the collapse exceedance probability in the probability range 0.75–1..

6. Conclusions

In this paper, a procedure for the definition of analytical fragility curves for multi-storey masonry buildings under tsunami actions to be used in huge areas, improving the approaches in the literature in the part regarding the assignment/assessment of the uncertainties, is proposed and discussed, contemporary verifying in which conditions the fragility lognormal distribution is reliable.

The study, particularized to the case of one-storey and three-storey

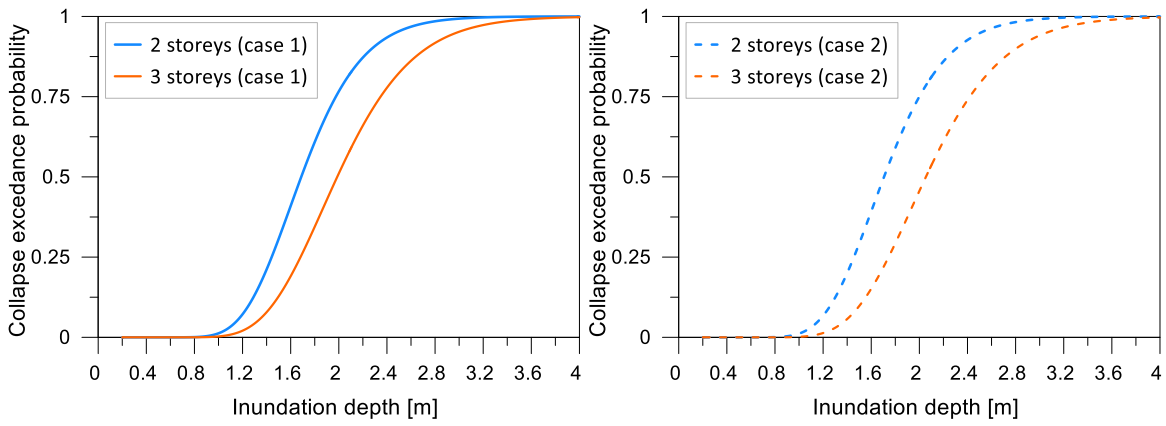

Fig. 20. Analytical collapse exceedance probability: a) comparison between 2 storeys and 3 storeys buildings characterized by the same strengths of masonry (case 1); b) comparison between 2 storeys and 3 storeys buildings characterized by the same strengths of masonry (case 2).

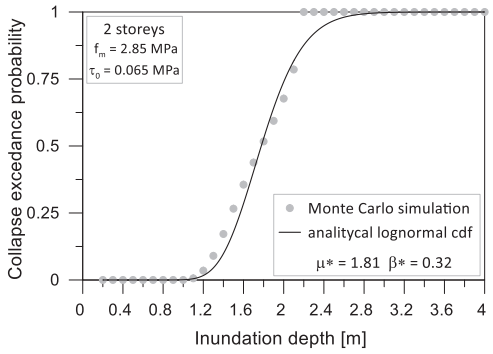

Fig. 21. Collapse exceedance probability in case of deterministic geometry.

masonry buildings typical of the Mediterranean area, has highlighted that:

1) assuming the probabilistic distribution of the variables involved in the structural capacity (geometry, mechanical characteristics, etc) and the probabilistic distribution of the random variables involved in the Tsunami demand (inundation depth and flow velocity) leads to a robust assessment of the probability of a damage state occurrence;
2) capacity and demand are strictly dependent by the probabilistic point of view, therefore the fragility assessment approaches based on the assumption of the independence of the uncertainties of demand and capacity may be unreliable;
3) using Monte Carlo simulation does not require a separate assessment of the uncertainties of capacity and demand for their following combination as currently proposed in the literature;
4) the results of the Monte Carlo simulation, in terms of probability of exceedance of a damage state, can be optimally fitted by analytical lognormal distribution curves, depending on mean and standard deviation of the logarithms of the inundation depths associated with the building damage state considered;
5) the rigorous evaluation of the uncertainties by the Monte Carlo simulation, and the good agreement between results of the Monte Carlo simulation and lognormal distribution curves, evidences the effectiveness of the strategy for obtaining the analytical fragility, not constrained to the assumption of probabilistic independence between capacity and demand;
6) the lognormal distribution of the fragility may fail in the case, provided in the literature, of deterministic assignment of the building geometry and probabilistic assumption of demand and structural mechanical characteristics; this underlines the appropriateness of the procedure discussed for large-scale evaluations characterized by a random variability of the building geometries.

The procedure, applied in the case of masonry buildings and resulted quick for large-scale evaluations because of the simplified model capacity used, is modifiable to be adapted to different building/structure typologies.

CRediT authorship contribution statement

Panagiotis G. Asteris: Conceptualization, Data curation, Investigation, Methodology. **Maria Concetta Oddo:** Conceptualization, Data curation, Formal analysis, Investigation, Writing – original draft. **Liborio Cavaleri:** Conceptualization, Data curation, Formal analysis, Funding acquisition, Investigation, Methodology, Supervision, Validation, Writing – original draft, Writing – review & editing.

Declaration of Competing Interest

The authors declare that they have no known competing financial interests or personal relationships that could have appeared to influence the work reported in this paper.

Acknowledgements

This study was carried out within the RETURN Extended Partnership and received funding from the European Union Next-Generation EU (National Recovery and Resilience Plan – NRRP, Mission 4, Component 2, Investment 1.3 – D.D. 1243 2/8/2022, PE0000005).

References

[1] Unesco/Intergovernmental Oceanographic Commission. 2009. Tsunami risk assessment and mitigation for the Indian Ocean: knowing your tsunami risk-and what to do about it. Unesco.
[2] Kelleher J. Rupture zones of large South American earthquakes and some predictions. J Geophys Res 1972;77:2087–103. https://doi.org/10.1029/JB077i011p02087.
[3] Herd DG, et al. The Great Tumaco, Colombia earthquake of 12 December 1979. Science 1981;211(4481):441–5.
[4] Hayashi Y. Tsunami disaster caused by 1993 earthquake in northern part of Japan sea. J Coast Res 1994;10(3):775–81.
[5] EEFIT. The Indian Ocean Tsunami of 26 December 2004: Mission Findings in SriLanka and Thailand. field report by the Earthquake Engineering Field Investigation Team (EEFIT), Institution of Structural Engineers; 2006. Available from: ⟨http://www.istructe.org/webtest/files/74/74b66946-020a-430d-a684-0f71ff0d2a23.pdf⟩.
[6] Roeber V, Yamazaki Y, Cheung KF. Resonance and impact of the 2009 Samoa tsunami around Tutuila, American Samoa. Geophys Res Lett 2010;37:L21604. https://doi.org/10.1029/2010GL044419.

[7] Fritz HM, Petroff CM, Catalan PA, et al. Field survey of the 27 February 2010 Chile Tsunami. Pure Appl Geophys 2011;168:1989–2010. https://doi.org/10.1007/s00024-011-0283-5.

[8] Otero LJ, Restrepo JC, Gonzalez M. Tsunami hazard assessment in the southern Colombian Pacific basin and a proposal to regenerate a previous barrier island as protection. Nat Hazards Earth Syst Sci 2014;14:1155–68. https://doi.org/10.5194/nhess-14-1155-2014.

[9] Goda K, Mori N, Yasuda T, Prasetyo A, Muhammad A, Tsujio D. Cascading geological hazards and risks of the 2018 Sulawesi Indonesia earthquake and sensitivity analysis of tsunami inundation simulations Katsuichiro. Front Earth Sci 2019. https://doi.org/10.3389/feart.2019.00261.

[10] Fritz HM, Mohammed F, Yoo J. Lituya Bay landslide impact generated mega-tsunami 50th anniversary. Pure Appl Geophys 2009;166:153–75. https://doi.org/10.1007/s00024-008-0435-4.

[11] Suppasri A, Mas E, Charvet I, Gunasekera R, Imai K, Fukutani Y, et al. Building damage characteristics based on surveyed data and fragility curves of the 2011 Great East Japan tsunami. Nat Hazards 2013;66:319–41. https://doi.org/10.1007/s11069-012-0487-8.

[12] Lagomarsino S, Giovinazzi S. Macroseismic and mechanical models for the vulnerability and damage assessment of current buildings. Bull Earthq Eng 2006;4:415–43.

[13] Silva V, Crowley H, Varum H, Pinho R, Sousa R. Evaluation of analytical methodologies used to derive vulnerability functions. Earthq Eng Struct Dyn 2014;43(2):181–204.

[14] Ioannou I, Douglas J, Rossetto T. Assessing the impact of ground-motion variability and uncertainty on empirical fragility curves. Soil Dyn Earthq Eng 2015;69:83–92.

[15] Cavaleri L, Di Trapani F, Ferrotto MF. A new hybrid procedure for the definition of seismic vulnerability in Mediterranean cross-border urban areas. Nat Hazards 2017;86:517–41.

[16] Asteris PG, Moropoulou, Skentou A, Apostolopoulou AD, Mohebkhah M, Cavaleri A, et al. Stochastic vulnerability assessment of masonry structures: concepts, modeling and restoration aspects. Appl Sci 2019;9(2):243. https://doi.org/10.3390/app9020243.

[17] Petrone C, Rossetto T, Goda K. Fragility assessment of a RC structure under tsunami actions via nonlinear static and dynamic analyses. Eng Struct 2017;136:36–53.

[18] Karafagka S, Fotopoulou S, Pitilakis K. Analytical tsunami fragility curves for seaport RC buildings and steel light frame warehouses. Soil Dyn Earthq Eng 2018;112:118–37.

[19] Medina S, Lizarazo-Marriaga J, Estrada M, Koshimura S, Mas E, Adriano B. Tsunami analytical fragility curves for the Colombian Pacific coast: a reinforced concrete building example. Eng Struct 2019;196:109309.

[20] Pitilakis K, Argyroudis S, Fotopoulou S, Karafagka S, Kakderi K, Selva J. Application of stress test concepts for port infrastructures against natural hazards. The case of Thessaloniki port in Greece. Reliab Eng Syst Saf 2019;184:240–57.

[21] Alam MS, Barbosa AR, Scott MH, Cox DT, Van de Lindt JW. Development of physics-based tsunami fragility functions considering structural member failures. J Struct Eng 2018;144(3):04017221.

[22] Suppasri A, Mas E, Koshimura S, Imai K, Harada K, Imamura F. Developing tsunami fragility curves from the surveyed data of the 2011 Great East Japan tsunami in Sendai and Ishinomaki Plains. Coast Eng J 2012;54(1):1250008-1. https://doi.org/10.1142/S0578563412500088.

[23] Suppasri A, Charvet I, Imai K, Imamura F. Fragility curves based on data from the 2011 Tohoku-oki tsunami in Ishinomaki city, with discussion of parameters influencing building damage. Earthq Spectra 2015;31(2):841–68.

[24] Macabuag J, Rossetto T, Ioannou I, Suppasri A, Sugawara D, Adriano B, et al. A proposed methodology for deriving tsunami fragility functions for buildings using optimum intensity measures. Nat Hazards 2016;84:1257–85. https://doi.org/10.1007/s11069-016-2485-8.

[25] Macabuag J, Raby A, Pomonis A, Nistor I, Wilkinson S, Rossetto T. Tsunami design procedures for engineered buildings: a critical review (Thomas Telford Ltd.) Proc Inst Civ Eng-Civ Eng 2018;Vol. 171(No. 4):166–78. https://doi.org/10.1680/jcien.17.00043.

[26] Foytong P, Ruangrassamee A, Lukkunaprasit P, Thanasisathit N. Behaviours of reinforced-concrete building under tsunami loading. IES J Part A Civ Struct Eng 2015;8(2):101–10. https://doi.org/10.1080/19373260.2015.1013998.

[27] Ferrotto MF, Cavaleri L. Masonry structures: a proposal of analytical generation of fragility functions for tsunami impact–Application to the Mediterranean coasts. Eng Struct 2021;242:112463.

[28] National Institute of Building Sciences. Direct physical damage–general building stock. HAZUS-MH Tech Man, Chapter 2004;5.

[29] FEMA. 2012. Guidelines for design of structures for vertical evacuation from Tsunamis. (FEMA P-646). FEMA P-646 Publ.

[30] ASCE/SEI 7–16 (American Society of Civil Engineers). 2017. Minimum design loads for buildings and other structures, Reston, Virginia.

[31] Triatmadja R, Nurhasanah A. Tsunami force on buildings with openings and protection. J Earthq Tsunami 2012;6(04):1250024.

[32] Robertson IN, Paczkowski K, Riggs HR, Mohamed A. Experimental investigation of tsunami bore forces on vertical walls. J Offshore Mech Arct Eng 2013;135(2):021601.

[33] Qi ZX, Eames I, Johnson ER. Force acting on a square cylinder fixed in a free-surface channel flow. J Fluid Mech 2014;756:716–27.

[34] Shafiei S, Melville BW, Shamseldin AY. Experimental investigation of tsunami bore impact force and pressure on a square prism. Coast Eng 2016;110:1–16.

[35] Foster ASJ, Rossetto T, Allsop W. An experimentally validated approach for evaluating tsunami inundation forces on rectangular buildings. Coast Eng 2017;128:44–57.

[36] Wüthrich D, Pfister M, Nistor I, Schleiss AJ. Experimental study on the hydrodynamic impact of tsunami-like waves against impervious free-standing buildings. Coast Eng J 2018;60(2):180–99.

[37] Wüthrich D, Pfister M, Nistor I, Schleiss AJ. Experimental study of tsunami-like waves generated with a vertical release technique on dry and wet beds. J Waterw, Port, Coast, Ocean Eng 2018;144(4):04018006.

[38] Wüthrich D, Pfister M, Nistor I, Schleiss AJ. Experimental study on forces exerted on buildings with openings due to extreme hydrodynamic events. Coast Eng 2018;140:72–86.

[39] Matsutomi H, Okamoto K. Inundation flow velocity of tsunami on land. Isl Arc 2010;19(3):443–57.

[40] Attary N, van de Lindt JW, Unnikrishnan VU, Barbosa AR, Cox DT. Methodology for development of physics-based tsunami fragilities. J Struct Eng 2017;143(5):04016223.

[41] Ministero delle Infrastrutture e dei Trasporti. 2018. Aggiornamento delle Norme Tecniche per le Costruzioni (NTC2018) (in Italian). Ministero delle Infrastrutture e dei Trasporti: Roma, Italy.

[42] Ministero delle Infrastrutture e dei Trasporti. 2019. Circolare 21 gennaio 2019 n. 7 CS LL. PP. Istruzioni per l'applicazione dell'aggiornamento delle 'Norme Tecniche per le Costruzioni di cui al DM 17/01/2018 (in Italian). Suppl. Ord. Alla GU n. 35 Del 11/2/19.

[43] Benfratello S, Cavaleri L, Papia M. Identification of stiffness, dissipation and input parameters of multi degree of freedom civil systems under unmeasured base excitations. Probabilistic Eng Mech 2009;24:190–8.

[44] Cavaleri L, Papia M. An output-only stochastic parametric approach for the identification of linear and nonlinear structures under random base excitations: advances and comparisons. Probabilistic Eng Mech 2014;35:11–21.

[45] Cima V, Tomei V, Grande E, Imbimbo M. Fragility curves for the seismic assessment of masonry buildings in historic centres prone to out-of-plane failure modes. Bull Earthq Eng 2024;22:1801–26.

[46] Van Rossum G. Python Programming Language. In: Proceedings of the USENIX annual technical conferencef 2007;41(1):1–36.